Acta Pharmacologica Sinica

www.nature.com/aps

ARTICLE

Helichrysetin inhibits gastric cancer growth by targeting c-Myc/PDHK1 axis-mediated energy metabolism reprogramming

Ping Wang[1], Jin-mei Jin[1], Xiao-hui Liang[1], Ming-zhu Yu[1], Chun Yang[1], Fei Huang[1], Hui Wu[1], Bei-bei Zhang[1], Xiao-yan Fei[2], Zheng-tao Wang[1], Ren Xu[3], Hai-lian Shi[1] and Xiao-jun Wu[1]

Helichrysetin (HEL), a chalcone isolated from *Alpinia katsumadai Hayata*, has an antitumor activity in human lung and cervical cancers. However, the inhibitory effect and underlying mechanism of HEL in gastric cancer have not been elucidated. Here, HEL significantly inhibited the growth of gastric cancer MGC803 cells in vitro and in vivo. HEL decreased expression and transcriptional regulatory activity of c-Myc and mRNA expression of c-Myc target genes. HEL enhanced mitochondrial oxidative phosphorylation (OXPHOS) and reduced glycolysis as evidenced by increased mitochondrial adenosine triphosphate (ATP) production and excessive reactive oxygen species (ROS) accumulation, and decreased the pPDHA1/PDHA1 ratio and Glyco-ATP production. Pyruvate enhanced OXPHOS after HEL treatment. c-Myc overexpression abolished HEL-induced inhibition of cell viability, glycolysis, and protein expression of PDHK1 and LDHA. PDHK1 overexpression also counteracted inhibitory effect of HEL on cell viability. Conversely, c-Myc siRNA decreased cell viability, glycolysis, and PDHK1 expression. NAC rescued the decrease in viability of HEL-treated cells. Additionally, HEL inhibited the overactivated mTOR/p70S6K pathway in vitro and in vivo. HEL-induced cell viability inhibition was counteracted by an mTOR agonist. mTOR inhibitor also decreased cell viability. Similar results were obtained in SGC7901 cells. HEL repressed lactate production and efflux in MGC803 cells. These results revealed that HEL inhibits gastric cancer growth by targeting mTOR/p70S6K/c-Myc/PDHK1-mediated energy metabolism reprogramming in cancer cells. Therefore, HEL may be a potential agent for gastric cancer treatment by modulating cancer energy metabolism reprogramming.

Keywords: helichrysetin; gastric cancer; c-Myc; PDHK1; energy metabolism reprogramming

Acta Pharmacologica Sinica (2022) 43:1581–1593; https://doi.org/10.1038/s41401-021-00750-0

INTRODUCTION

Gastric cancer is one of the most common gastrointestinal cancers and the third leading cause of cancer-related mortality, mostly in Asia [1–3]. Surgical resection is the main therapeutic regimen for most gastric cancer patients, but the 5-year overall survival rate is less than 30% [4–6]. Chemotherapy has been widely used for the treatment of middle- and late-stage gastric cancers [7, 8], which is accompanied by serious adverse effects such as cardiovascular toxicity, gastrointestinal toxicity, hemotoxicity, nephrotoxicity, and neurotoxicity. These side effects compromise clinical efficacy and reduce the life quality of patients [9–12]. Therefore, development of new chemotherapeutic drugs with less adverse effects is needed for gastric cancer patients.

Cancer cells proliferate and grow by reprogramming their energy metabolism [13, 14]. Therefore, cancer is regarded as a metabolic disease [15]. Gastric cancer cells obtain energy mainly via glycolysis to produce energy and intermediate metabolites to synthesize substances required for proliferation and growth. Pyruvate dehydrogenase (PDH), a gatekeeping enzyme of aerobic glycolysis and the mitochondrial tricarboxylic acid (TCA) cycle, is responsible for catalyzing pyruvate into acetyl-CoA for the TCA cycle. Pyruvate dehydrogenase kinase 1 (PDHK1) is the switch enzyme in mitochondria of cancer cells to modulate metabolism reprogramming. It inhibits the activity of PDH by phosphorylating the latter, which reduces the formation of acetyl-CoA from pyruvate for the TCA cycle, thereby promoting pyruvate to produce lactic acid and acidify the tumor microenvironment through aerobic glycolysis via lactate dehydrogenase (LDHA). This finally promotes tumor cell proliferation, survival, and growth [16–21]. Therefore, PDHK1 is regarded as a target for anticancer drug development.

c-Myc, which is highly expressed in gastric cancer [22, 23], is a major regulator of cancer cell energy metabolism [24]. It regulates the expression of PDHK1 by binding to the PDHK1 promoter [25]. c-Myc also modulates glucose uptake, aerobic glycolysis, and lactate acid production and efflux [25–29] by regulating the

[1]Shanghai Key Laboratory of Compound Chinese Medicines, The Ministry of Education (MOE) Key Laboratory for Standardization of Chinese Medicines, The SATCM Key Laboratory for New Resources & Quality Evaluation of Chinese Medicine, Research Center of Shanghai Traditional Chinese Medicine Standardization, Institute of Chinese Materia Medica, Shanghai University of Traditional Chinese Medicine, Shanghai 201203, China; [2]Longhua Hospital, Shanghai University of Traditional Chinese Medicine, Shanghai 200032, China and [3]Markey Cancer Center, Department of Pharmacology and Nutritional Sciences, University of Kentucky College of Medicine, Lexington, KY, USA
Correspondence: Hai-lian Shi (shihailian2003@163.com) or Xiao-jun Wu (xiaojunwu320@126.com)
These authors contributed equally: Ping Wang, Jin-mei Jin

Received: 4 January 2021 Accepted: 20 July 2021
Published online: 30 August 2021

Table 1. Primers used in qPCR analysis.

Genes	Forward primer	Reverse primer
c-Myc	5′-TCGGATTCTCTGCTCTCCTC-3′	5′- TCGGTTGTTGCTGATCTGTC -3′
PDHK1	5′- GATGTGAATGGGCAGTTAGT-3′	5′-AGGAATAGTGGGTTAGGTGAG-3′
LDHA	5′-TGGAGTGGAATGAATGTTG-3′	5′- GATGTGTAGCCTTTGAGTTTG-3′
LDHB	5′- GAAGGAGGAAGAAGCACA-3′	5′-GCACAAGGACAAGTAGGG -3′
GAPDH	5′- GCACCGTCAAGGCTGAGAAC-3′	5′- TGGTGAAGACGCCAGTGGA-3′

expression of PDHK1, glucose transporters (GLUTs) such as GLUT1, 3, 4, hexokinase 2 (HK2), and muscle phosphofructokinase, lactate dehydrogenase A (LDHA), and monocarboxylate transporters (MCTs) such as MCT1 and MCT4, which leads to energy metabolism reprogramming [25, 27, 28, 30]. c-Myc expression is regulated by the PI3K/PTEN/AKT pathway in an mTOR-dependent manner [31–33].

Helichrysetin (HEL), a chalcone isolated from *Alpinia katsumadai Hayata*, has prominent antitumor activities [34–39]. For example, HEL induces apoptosis and cell cycle arrest in human lung adenocarcinoma A549 cells [38] and causes DNA damage that triggers JNK-mediated apoptosis in human cervical cancer Ca Ski cells [39]. However, the effect and mechanism of HEL in gastric cancer progression have been rarely investigated. In the present study, we found that HEL significantly inhibited the growth of gastric cancer cell line MGC803 in vivo and in vitro, which was mediated by reprogramming cancer energy metabolism through inhibition of the mTOR/c-Myc/PDHK1 pathway. These findings may facilitate clinical application of HEL to gastric cancer treatment.

MATERIALS AND METHODS

Chemicals

HEL (>95% purity) was supplied by Prof. Jingshan Shen (Shanghai Institute of Materia Medica, Chinese Academy of Sciences, Shanghai, China). The 5-Fluorouracil (5-Fu) (#MB1273) was purchased from Meilunbio (China). Sodium pyruvate (#11360070) was purchased from Gibco (USA).

Cell culture

Human gastric cancer cell line MGC803 and human colon carcinoma cell line HCT-8 were obtained from the Type Culture Collection of Chinese Academy of Sciences (Shanghai, China) and maintained in RMPI-1640 medium (Thermo Fisher Scientific, Inc.) supplemented with 10% FBS, 100 U/mL penicillin, and 100 U/mL streptomycin at 37 °C in a humidified atmosphere with 5% CO_2. Human breast cancer cell line MDA-MB-231 was also provided by the Type Culture Collection of Chinese Academy of Sciences and cultured in DMEM with 10% FBS, 100 U/mL penicillin, and 100 U/mL streptomycin. Human gastric cancer cell line AGS was cultured in HAM's F-12 medium with 10% FBS, 100 U/mL penicillin, and 100 U/mL streptomycin. MGC 803 cells stably overexpressing c-Myc were cultured in RMPI-1640 medium with 10% FBS, 100 U/mL penicillin, 100 U/mL streptomycin, and 2 μg/mL puromycin.

Cell viability assay

Human cancer cells were seeded in 96-well plates and grown overnight. After treatment with HEL at various concentrations (5, 10, 20, 40, 80, 120, 160, and 200 μM) for 48 h, the cells were incubated with 20 μL/well CCK-8 reagent (Cell Counting Kit-8, #CK04, Dojindo Laboratories, Japan) and at 37 °C for another 1 h. The *OD* value of the culture medium at 450 nm was measured on a microplate reader (Varioskan Flash, Thermo, USA). The cell viability rate was calculated as follows: (absorbance of drug-treated sample/absorbance of control sample) ×100%.

Western blot analysis

A total of 30 μg protein from each sample was separated by SDS-PAGE (8, 10, or 12%) and then transferred onto a PVDF membrane by wet transfer. After blocking with 5% (*w*/*v*) bovine serum albumin (BSA) in PBS, the membrane was incubated with primary antibodies against Ki67 (1:1000, sp6, #ab16667, Abcam, USA), Bcl-2 (1:1000, 50E3, #2870, CST, USA), Bax (1:1000, D2E11, #5023, CST), Cleaved caspase-3 (1:1000, 5A1E, #9664, CST), LDHA (1:1000, c28H7, #3558, CST), LDHB (1:1000, 60H11, #ab85319, Abcam), PDHK1 (1:1000, C47H1, #3820, CST), c-Myc (1:5000, Y69, #ab32072, Abcam), PI3K (1:1000, #4257 S, CST), p-PI3K p85 (Tyr458)/p55 (Tyr199) (1:500, #4228, CST), Akt (1:1000, #4685S, CST), p-AKT (S473) (1:1000, D9E, #4060, CST), mTOR (1:1000, Y391, #ab32028, Abcam), p-mTOR (1:500, D9C2, #5536, CST), p70S6K (1:1000, #9202, CST), p-p70S6K (1:1000, #9234S, Abcam), Nrf2 (Santa Cruz, #sc-722, 1:1000), NQO1 (Santa Cruz, #sc-32793, 1:1000), HO-1 (Santa Cruz, #sc-136960, 1:1000), PDP2 (1:10000, #ab133982, Abcam), pPDHA1 (1:10000, #AP1062, Sigma, USA), PDHA1 (1:10000, #18068-I-AP, Proteintech, USA), GAPDH (1:1000, D16H11, #5174, CST), LaminB1 (1:3000, #6581-1, Epitomics, USA), and flag (1:1000, #F1804, Sigma) at 4 °C overnight. Consequently, the membranes were incubated with horseradish peroxidase (HRP)-conjugated secondary antibodies for 1 h at room temperature (RT). The target protein bands were visualized with an ECL-prime kit (Millipore, #WBKLS0500, USA) in a Tanon-5200 instrument (20182351, Tanon, China). Quantification of the target protein was normalized to glyceraldehyde-3-phosphate dehydrogenase (GAPDH) within the same sample.

Real-time quantitative PCR (qPCR)

Total RNA was extracted using Trizol reagent (Thermo) in accordance with the manufacturer's instructions. cDNA was reverse transcripted from 2 μg RNA using a RevertAid First Strand cDNA Synthesis Kit (#K1622, Thermo Scientific, USA). Real-time qPCR was performed using SYBR Premix EX Taq (Roche, USA) on a Quant Studio 6 Flex System (Life Technologies, USA) under the following conditions: 95 °C, 10 min; 40 cycles (95 °C, 15 s; 60 °C, 60 s); 95 °C, 15 s; 60 °C, 1 min; 95 °C, 15 s. Quantification of target gene expression was performed by the $2^{-\Delta\Delta Ct}$ method. Relative mRNA expression of target genes was normalized to GAPDH in the same sample. The sequences of primers (GeneRay, China) are listed in Table 1.

EdU staining

Cells were seeded at a density of 0.8×10^5 cells/well on a 96-well plate and allowed to adhere overnight. EdU staining was carried out using a kFluor488 Click-iT EdU imaging kit (#KGA331-100, KeyGenBiotech, China). In brief, MGC803 cells treated with HEL (0, 1, and 5 μM) for 24 h were incubated with a 10 μM EdU for 2 h. Then, the cells were fixed in 4% PFA for 20 min, followed by neutralization with a 2 mg/mL glycine solution for 5 min. After permeabilization with 0.5% Triton X-100 for 20 min, the cells were incubated with the Click-iT reaction mixture for 30 min and then counterstained with 5 μg/mL Hoechst 33342. Images were captured by fluorescence microscopy. Data were analyzed using ImageJ software.

Mitochondrial membrane potential (MMP) measurement
MMP of MGC 803 cells was measured using the fluorescent probe JC-1 (#sc-364116, Santa Cruz). Cells treated with 20 μM HEL for various times were rinsed with HBSS (#14025-092, Gibco) and incubated with 10 μM JC-1 for 30 min at 37 °C. Then, the cells were rinsed with HBSS. Fluorescence intensities of JC-1 monomers and aggregates were detected under different conditions [Ex (λ) 485 nm, Em (λ) 530 nm for monomers; Ex (λ) 530 nm, Em (λ) 590 nm for aggregates] on the Varioskan Flash microplate reader. Fluorescence images of the cells were obtained under a fluorescence microscope (IX81, Olympus, Japan).

Cell apoptosis assay
Gastric cancer cells were seeded in six-well plates at a density of 7.5×10^4 cells/well and allowed to adhere overnight. After serum starvation for 24 h, the cells were incubated with various concentrations of HEL (10, 20, and 40 μM) in medium with 10% FBS for another 24 h. The cells were subsequently harvested by trypsinization and washed twice with 1× Annexin V binding buffer. After resuspension in 1× Annexin V binding buffer, the cells were stained with a 1× Annexin V and PI solution. Fluorescence of the cells was analyzed on a Guava flow cytometer (Millipore).

c-Myc luciferase reporter assay
MGC803 cells were seeded in 48-well plates (1×10^5 cells/well) and allowed to adhere overnight. At 70% confluence, the cells were transiently transfected with 500 ng/well pGL4[luc2P/Myc/Hygro] Vector (#CS180201, Promega, USA) and 10 ng/well renilla luciferase plasmid using Lipofectamine® LTX & PLUS™ Reagent (#15338-100, Thermo) for 8 h. Then, the cells were incubated with HEL (0, 10, 20, and 40 μM) for 24 h. Finally, the cells were harvested and subjected to a luciferase activity assay using a Dual-Luciferase® Reporter Assay system (#E1910, Promega) in accordance with the manufacturer's instructions.

Glucose uptake assay
Glucose uptake was assessed using fluorescent glucose analog 2-[N-(7-nitrobenz-2-oxa-1, 3-diaxol-4-yl) amino]-2-deoxyglucose (2-NBDG; #N13195, Invitrogen, USA). MGC803 cells were seeded in 60-mm dishes (4×10^5 cells/dish) 1 day before the experiment. Then, the cells were treated with 20 μM HEL for 15 h. The medium was replaced with a 100 μM 2-NBDG solution without glucose and sodium pyruvate, followed by incubation for 45 min. The cells were then harvested by trypsinization and subjected to fluorescence analysis. The fluorescence intensity was measured on the Varioskan Flash microplate reader [Ex (λ) 535 nm, Em (λ) 587 nm]. All data were normalized to the cell number and the values of the treatment groups were expressed as percentages of the control group.

L-Lactate assay
An L-Lactate Assay Kit (#700510, Cayman, USA) was used to measure extracellular and intracellular *L*-lactate contents of gastric cancer cells. All reagents were prepared in accordance with the manufacturer's instructions. MGC803 cells were seeded in 60-mm dishes (4×10^5 cells/dish) 1 day before the experiment. After growing to the appropriate confluence, the cells were treated with 20 μM HEL for 15 h. Then, the medium was replaced with drug-free 0.5% FBS-containing fresh medium and the cells were cultured for another 4 h. The supernatant and cells were collected by centrifugation at $2000 \times g$ for 10 min at 4 °C, and used to determine the extracellular and intracellular *L*-lactate contents, respectively, in accordance with the manufacturer's manual. The fluorescence intensity was measured on the Varioskan Flash microplate reader [Ex (λ) 535 nm, Em (λ) 590 nm]. The *L*-lactate concentrations of the samples were calculated in accordance with the formula in the manufacturer's instructions. All data were normalized to the cell number.

Cell metabolism assays
A Mito Stress Test Kit (#103015-100, Agilent, USA) was used to measure the oxygen consumption rate (OCR). A Glycolytic Rate Assay Kit (#103344-100, Agilent) was used to measure the glycolytic proton efflux rate (GlycoPER). An Agilent Seahorse XF Real-Time ATP Rate Assay Kit (#103592-100, Agilent) was used to measure the ATP production rates of mitochondrial oxidative phosphorylation and glycolysis in gastric cancer cells. Before metabolism measurement, the probe plate was hydrated with HPLC-grade water in a CO_2-free incubator. Phenol red-free assay solution (10 mM glucose, 2 mM glutamine, 1 mM pyruvate, and 5 mM HEPES) was kept in a 37 °C CO_2-free incubator. Then, HPLC-grade water in the hydration plate was replaced with calibration solution and kept in the 37 °C CO_2-free incubator. Gastric cancer cells were seeded in Seahorse XF96 V3 PS Cell Culture Microplates (#101085-004, Agilent) at the density of 4×10^4 cells/well for measurement of OCR and ECAR or 7500 cells/well for measurement of ATP production rates, and allowed to adhere overnight. Then, the cells were incubated with 20 μM HEL for 0, 6, 9, 12, and 15 h. The cell culture medium was replaced with phenol red-free assay solution and the plate was placed in the 37 °C CO_2-free incubator for 1 h. Finally, OCR, ECAR, and ATP production rates were determined and analyzed on a Bioscience XF96 Extracellular Flux Analyzer (Seahorse Bioscience, North Billerica, MA, USA) in accordance with the manufacturer's instructions.

To measure GlycoPER, Rot/AA (inhibitors of the mitochondrial electron transport chain) and 2-deoxy-*D*-glucose (inhibitor of glycolysis) (Seahorse Bioscience) were added in accordance with the manufacturer's instructions.

To measure OCR, oligomycin, FCCP, and Rot/AA (Seahorse Bioscience) were added in accordance with the manufacturer's instructions.

To determine adenosine triphosphate (ATP) production, oligomycin and a mix of rotenone and antimycin A (Seahorse Bioscience) were added in accordance with the manufacturer's instructions.

ROS measurement
A Reactive Oxygen Species Assay Kit (#50101ES01, Yeasen, China) was used to determine the intracellular ROS level by measuring the change in fluorescence intensity of the fluorescent dye 2,7-dichloro-dihydrofluorescein diacetate (DCFH-DA) because DCFH is oxidized into fluorescent dichlorofluorescein (DCF) in the presence of ROS. MGC803 cells were cultured in a 96-well solid white polystyrene microplate (1×10^4 cells/well). After treatment with 20 μM HEL for 18 and 24 h, the cells were incubated with 10 μM DCFH-DA in phenol-free RPMI-1640 medium at 37 °C for another 30 min. Excess dye was removed and the cells were rinsed with prewarmed HBSS. Fluorescence of the cells was detected immediately on the Varioskan Flash microplate reader [Ex (λ) 485 nm, Em (λ) 535 nm].

Establishment of a c-Myc-overexpressing cell line
c-Myc overexpression lentiviral vector (LV-c-Myc, 2×10^8 TU/mL) and an empty GV358 vector (LV-CON, 1×10^9 TU/mL) were provided by Genechem (China). To establish a stably transfected cell line, MGC803 cells were seeded in a T-25 culture flask and allowed to attach for 24 h. MGC803 cells at 80% confluence were infected with the lentiviruses at 20 MOI in enhanced infection solution (ENi.S, #REVG0002, Genechem) with 5 μg/mL polybrene (#REVG0001, Genechem) for 8 h. The transfected cells were harvested and expanded in a T-100 culture flask. For the next week, the transfected cells were cultured in cell culture medium with puromycin (2.5 μg/mL, Sigma). Surviving cells that stably overexpressed c-Myc were maintained in medium with 1.25 μg/mL puromycin.

Transient transfection

At 60%–80% confluence, MGC803 cells were transiently transfected with GV230-PDHK1 (GeneChem) or GV230 plasmids using Neofect DNA transfection reagent (Neofect Beijing Biotech, China). Twenty-four hours later, the cells were treated with or without 20 μM HEL for another 24 h. Then, the cells were subjected to CCK-8 assays.

Animals and treatments

Male nude mice at 4 weeks of age were obtained from Shanghai Laboratory Animal Center of Chinese Academy of Science (Shanghai, China) and housed in a 12 h light/dark cycle at room temperature (25 ± 1 °C) and humidity (60% ± 10%) with free access to food and water. All animal experiments were carried out in accordance with protocols approved by the Animal Ethics Committee of Shanghai University of Traditional Chinese Medicine (SZY20160914), which complies with international rules and policies for laboratory animal use and care as stated in the European Community guidelines (EEC Directive of 1986; 86/609/EEC).

After 1 week of acclamation, each nude mouse was injected subcutaneously with 5×10^6 MGC803 cells. Body weights of the nude mice and tumor volumes were measured every 3 days. When the tumor volume reached ~50 mm^3, the mice were randomly divided into five groups: control, HEL (3, 10, and 30 mg/kg), and 5-Fu. Mice in control and HEL (3, 10, and 30 mg/kg every day) groups were intraperitoneally injected with physiological saline or HEL (3, 10, and 30 mg/kg) daily. Mice in the 5-Fu group were intraperitoneally injected with 50 mg/kg 5-Fu twice a week. The tumor volume was calculated by the following formula: [length × $(width)^2$]/2. After drug administration for 21 days, nude mice were sacrificed and the tumor tissues were harvested and divided equally into three parts. One portion of the tumor tissues was fixed in 4% polyformaldehyde, and the other two portions were stored at −80 °C for further analysis.

Hematoxylin and eosin (H&E) staining

H&E staining was conducted to assess pathological changes of tumor tissues in accordance with a previously described procedure [40]. Images were captured under a VS120 Virtual Slide Scanner (Olympus, Japan).

Immunohistochemistry (IHC)

IHC was performed in accordance with previously described protocols [41–43]. In brief, tumor tissue sections (5-μm thick) were deparaffinized with xylene and rehydrated in gradient alcohol solutions (anhydrous, 95% and 75%). The sections were placed in sodium citrate as an antigen retrieval solution and boiled in a microwave oven for 10 min. After washing three times in PBS, the sections were incubated with 3% H_2O_2 for 25 min at room temperature (RT) to block endogenous peroxidase. Then, they were incubated with 3% BSA blocking solution for 30 min, followed by incubation with a primary antibody against Ki67 overnight at 4 °C. Subsequently, the sections were incubated for 50 min at RT with a secondary antibody conjugated with HRP. After the development reaction with DAB, the sections were counterstained with hematoxylin. Ki67 proteins were stained brown and cell nuclei were stained blue. Images were captured under the VS120 Virtual Slide Scanner.

TUNEL assay

A TUNEL assay was performed with a TUNEL kit (#11684817910, Roche) in accordance with a previously described method with slight modifications [44]. Briefly, tumor tissue sections (5-μm thick) were deparaffinized with xylene and rehydrated in gradient alcohol solutions (anhydrous, 95% and 70%). Consequently, they were incubated with proteinase K (40 μg/mL) and permeabilized with 0.1% Triton X-100. After incubation with a mixture of reagent 1 (TdT) and reagent 2 (dUTP with FITC), the sections were counterstained with DAPI for 10 min. Images were captured under the VS120 Virtual Slide Scanner.

Statistical analysis

All data are presented as mean ± standard deviation. Differences between two groups were analyzed by the Student's *t*-test. Differences among more than two groups were analyzed by one-way ANOVA with Dunnett's or Turkey's test using GraphPad 5.0 software (La Jolla, CA, USA). $P < 0.05$ was considered statistically significant.

RESULTS

HEL decreases viability of MGC803 and SGC7901 cells by inhibiting c-Myc

MGC803 and AGS cells are human gastric cancer cells, HCT-8 cells are human colon carcinoma cells, and MDA-MB-231 cells are human breast cancer cells. Although they are all human cancer cells, they are from different tissues. After treatment for 48 h, HEL significantly reduced the viability of MGC803, AGS, MDA-MB-231, and HCT-8 cells with IC_{50} values of 16.07, 28.02, 86.43, and 108.7 μM, respectively (Fig. 1b). HEL had the best inhibitory effect on the viability of gastric cancer cell line MGC803, which suggested HEL had specificity for gastric cancer cells. Therefore, the following experiments were mainly performed with gastric cancer cell lines MGC803 cells and SGC7901 cells.

As shown in Fig. 1c, d, after treatment for 24 h, HEL at both 1 and 5 μM significantly decreased the number of EdU-positive cells ($P < 0.001$), which indicated its inhibitory effect on cell proliferation. At 10, 20, and 40 μM, HEL increased the apoptotic rates of MGC803 cells to 10.70%, 34.07%, and 63.15%, respectively, compared with control cells (Fig. 1e, f). Furthermore, as shown in Fig. 1g, h, HEL increased the protein expression of cleaved caspase 3 (20 and 40 μM, $P < 0.05$ and $P < 0.001$) and reduced protein expression of Bcl-2 (40 μM, $P < 0.05$) in MGC803 cells, but had no significant effect on the protein expression of Bax. These results suggested that HEL suppressed the growth of MGC803 cells, probably by simultaneously inhibiting cell proliferation and promoting apoptosis.

To explore the possible underlying mechanism of HEL in gastric cancer growth, the effects of HEL on transcriptional activity and expression of c-Myc were examined in MGC803 cells. As shown in Fig. 1i, HEL (10, 20, and 40 μM) significantly decreased c-Myc response element-controlled luciferase activity ($P < 0.001$). Moreover, HEL treatment, especially at high concentrations (20 and 40 μM) significantly inhibited the expression of c-Myc at both mRNA and protein levels (Fig. 1j–l; $P < 0.05$, $P < 0.01$, or $P < 0.001$). To confirm the role of c-Myc in the inhibitory effect of HEL, we established a stable cell line that overexpressed Flag-c-Myc (Fig. 1m). Compared with control cells, the inhibitory effect of HEL on the c-Myc-overexpressing MGC803 cells was significantly weaker (Fig. 1n; $P < 0.05$).

In SGC7901 cells, HEL also significantly inhibited viability with an IC_{50} value at 24 h of 31.8 μM (Fig. S3). HEL also significantly suppressed the protein expression of c-Myc in SGC7901 cells (Fig. S5a, b). c-Myc overexpression also significantly reversed HEL-induced inhibition of viability in SGC7901 cells (Fig. S5e).

These results robustly implicated that c-Myc plays a key role in the inhibitory effect of HEL on gastric cancer cell growth.

HEL modulates energy metabolism reprogramming in MGC803 cells

c-Myc triggers transcription of proteins that are closely associated with energy metabolism. To investigate whether HEL modulated energy metabolism in MGC803 cells, we examined the effect of HEL on the expression of PDHK1, LDHA, and LDHB. As shown in Fig. 2a–c, HEL (20 μM) significantly reduced the mRNA and protein

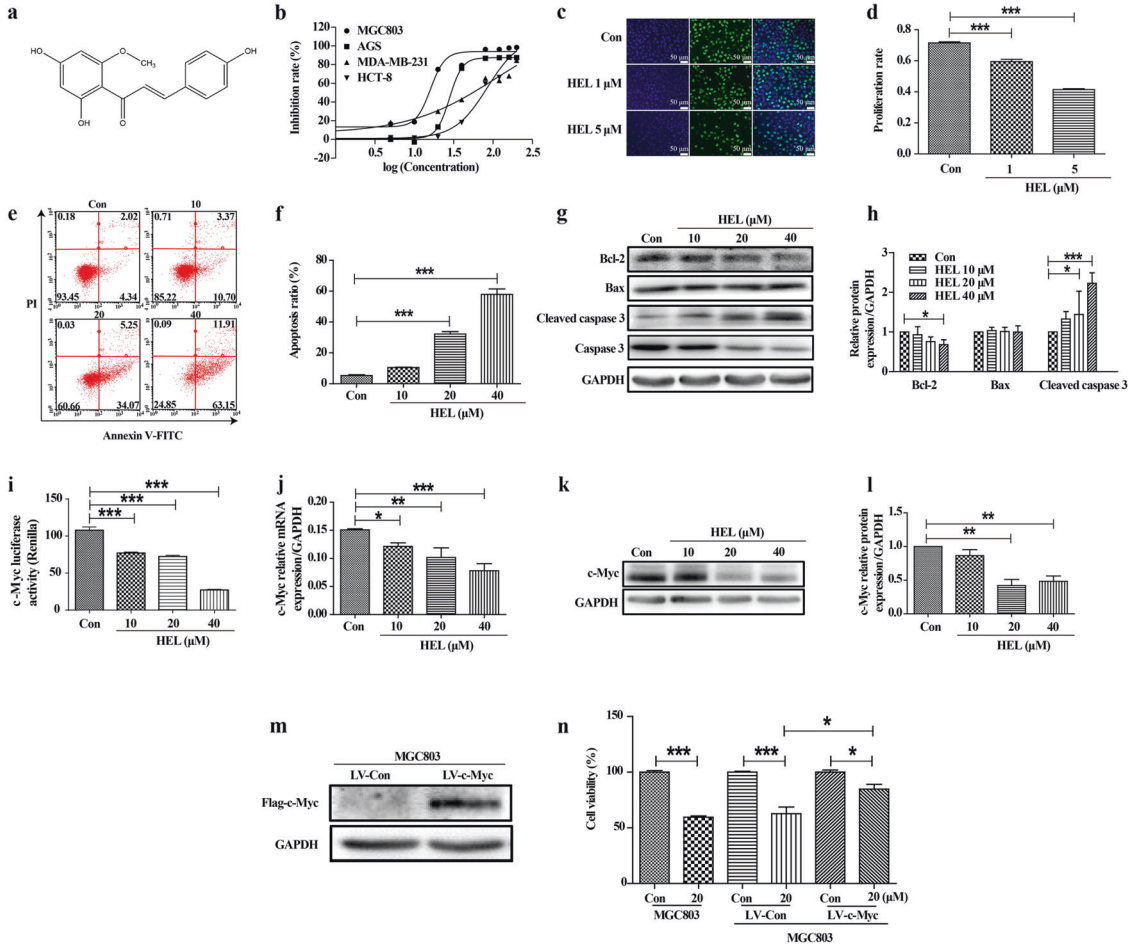

Fig. 1 HEL inhibits cell viability of MGC803 cells by inhibiting c-Myc. a Chemical structure of HEL. **b** Dose-response curves of MGC803, AGS, MDA-MB-231 and HCT-8 cell lines treated with various concentrations of HEL for 48 h. **c**, **d** EdU staining of MGC803 cells treated with HEL for 24 h. **e**, **f** Annexin V-FITC/PI staining of MGC803 cells treated with HEL. **g**, **h** Protein expression of Bcl-2, Bax and cleaved caspase 3 after HEL treatment for 24 h. **i** c-Myc luciferase reporter assay of MGC803 cells after HEL treatment for 24 h. **j** mRNA expression of c-Myc after HEL treatment for 24 h. **k**, **l** Protein expression of c-Myc after HEL treatment for 24 h. **m** c-Myc-flag overexpression in MGC 803 cells transfected with LV-c-Myc plasmid. **n** Cell viability of MGC803 cells transfected with empty vector (LV-Con) and c-Myc vector (LV-c-Myc) after HEL treatment for 24 h. Data are shown as mean ± SD; $^{*}P < 0.05$, $^{**}P < 0.01$; $^{***}P < 0.001$, compared with control. $n \geq 3$. Scale bar, 50 μm.

expression of PDHK1 and LDHA but only decreased the mRNA level of LDHB. HEL (20 μM) significantly decreased the protein expression of pyruvate dehydrogenase phosphatase (PDP) 2 and the ratio of p-PDHA1/PDHA1 (Fig. 2b, c). To assess the effect of HEL on energy metabolism while excluding bias caused by cell injury/death, the time-course effects of HEL on MMP and cell viability was measured. As shown in Fig. 2d–f, HEL treatment for less than 15 h had no obvious inhibitory effect on MMP and viability of MGC803 cells. Thus, in further experiments, the effect of HEL on real-time energy metabolism was examined at 0, 6, 9, 12, and 15 h. As displayed in Fig. 2g, h, HEL significantly enhanced the basal respiration, maximal respiration, spare capacity, proton leak, and ATP production in MGC 803 cells after treatment for 6, 9, 12, and 15 h ($P < 0.05$, $P < 0.01$, and $P < 0.001$), and the effect reached the peak at 9 h, which indicated HEL significantly enhanced mitochondrial oxidative phosphorylation (OXPHOS). Furthermore, as shown in Fig. 2i, j, after HEL treatment for 6, 9, 12, and 15 h, basal and compensatory glycolysis were reduced significantly ($P < 0.05$ and $P < 0.001$), which indicated HEL greatly mitigated glycolysis. Moreover, the glucose uptake, and extracellular and intracellular lactate contents of MGC803 cells treated with HEL (20 μM) were examined. As shown in Fig. 2k–m, compared with control cells, HEL treatment for 15 h did not change the glucose uptake of the cells. However, extracellular and intracellular *L*-lactate contents were decreased simultaneously ($P < 0.01$ and $P < 0.001$). These results indicated that HEL reversed energy metabolism reprogramming in MGC803 cells.

The elevated mitochondrial OXPHOS increased mito-ATP. Consistent with the above results, as shown in Fig. 3a, b, HEL increased mito-ATP production through mitochondrial OXPHOS, but decreased glyco-ATP production through glycolysis ($P < 0.01$ and $P < 0.001$). Mitochondria is the main source of ROS, which is a by-product of mitochondrial OXPHOS. HEL (20 μM) significantly increased the ROS level after treatment for 18 and 48 h (Fig. 3c, $P < 0.001$). When *N*-acetyl-cysteine (NAC; ROS scavenger; 5 mM) was added, the elevated ROS level induced by HEL (20 μM) was diminished (Fig. 3d). Correspondingly, the inhibitory effect of HEL on the viability of MGC803 cells was decreased (Fig. 3e).

Pyruvate (32 μM) treatment (9 h) significantly further increased the basal respiration, maximal respiration, spare capacity, proton leak, and ATP production of HEL-treated MGC 803 cells, which indicated that HEL promoted pyruvate entry into mitochondria for OXPHOS in MGC803 cells (Fig. 3f, g).

Nuclear factor-erythroid 2-related factor 2 (Nrf2) is a stress-response transcription factor that modulates the expression of antioxidant defense genes, such as NAD(P)H quinone oxidoreductase I (NQO1) and hemeoxygenase 1 (HO-1), by binding to antioxidant-response elements in the promoter region of NQO1

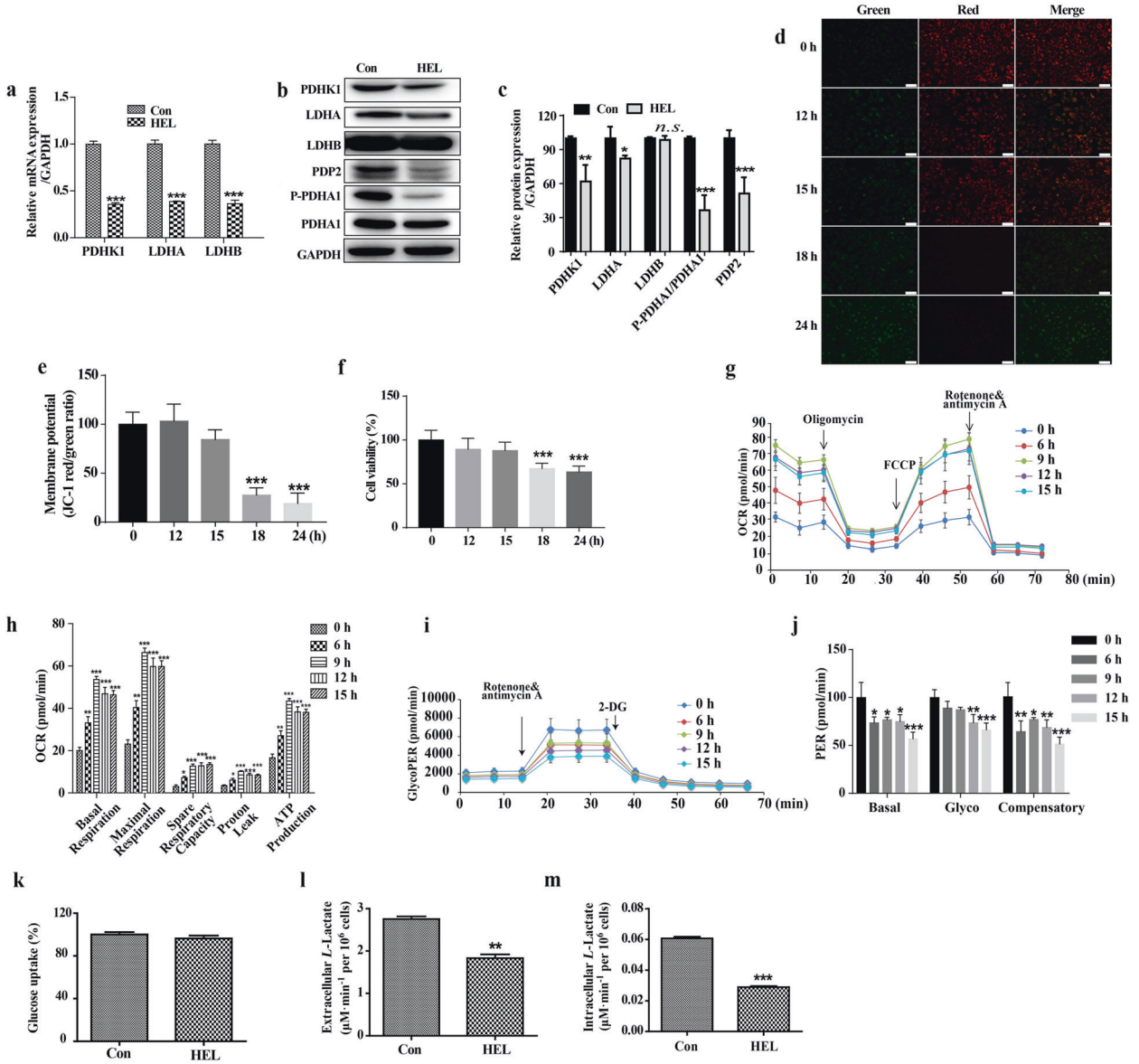

Fig. 2 HEL modulates energy metabolism reprogramming of MGC803 cells. a mRNA expression of PDHK1, LDHA, and LDHB in MGC803 cells after HEL treatment for 24 h. **b**, **c** Protein expression of PDP2, pPDHA1, PDHA1, PDHK1, LDHA, and LDHB in MGC803 cells after HEL treatment for 24 h. **d**, **e** MMP of MGC cells after HEL treatment for different time points. **f** Cell viability of MGC803 cells after HEL treatment for different time points. **g**, **h** Oxygen consumption rates (OCR) of MGC803 cells after HEL treatment for 0, 6, 9, 12, and 15 h. **i**, **j** Glycolytic rates of MGC803 cells after HEL treatment for 0, 6, 9, 12, and 15 h. **k** Glucose uptake ability of after HEL treatment for 15 h. **l**, **m** Extracellular and intracellular *L*-lactate contents of MGC803 cells after HEL treatment for 15 h. Data are shown as mean ± SD; **P* < 0.05, ***P* < 0.01; ****P* < 0.001, compared with control. $n \geq 3$. Scale bar, 50 μm.

and HO-1 under stress [45–48]. Activation of the Nrf2 defense system reduces ROS accumulation [49]. Keap1 inhibits translocation of Nrf2 into the nucleus to regulate its target genes that encode various antioxidant proteins and metabolic enzymes (phase II detoxifying enzymes) by binding to Nrf2 to form the Keap1–Nrf2 complex [50]. To investigate whether HEL weakened the ROS scavenging system in MGC803 cells, the protein expression of Keap1, Nrf2, HO-1, and NQO-1 were examined. Unexpectedly, the expression levels of Nrf2, HO-1, and NQO-1 were significantly upregulated, while that of Keap1 was reduced after HEL treatment (Fig. 3h, i, $P < 0.05$, $P < 0.01$, and $P < 0.001$). HEL also enhanced Nrf2 nuclear translocation in a time-dependent manner (Fig. 3j, k). These results indicated the enhanced mitochondrial OXPHOS induced by HEL may account for the over-accumulation of ROS and activation of the Nrf2 defense system by HEL could explain why HEL only induced a small increase of ROS in MGC803 cells.

In SGC7901 cells, HEL showed no significant inhibition of cell viability at 3–12 h and significantly suppressed the viability of SGC7901 cells as early as 24 h (Fig. S3b). HEL significantly induced ROS accumulation as early as 3 h after treatment (Fig. S3c). Furthermore, as shown in Fig. S4, HEL significantly reduced glycoPER after treatment for 9 and 12 h (Fig. S4a, b) and enhanced OCR after treatment for 6 and 9 h (Fig. S4c, d).

HEL modulates energy metabolism reprogramming through the c-Myc/PDHK1 axis. c-Myc is involved in energy metabolism by regulating the expression of energy metabolism-associated genes, and therefore we further investigated whether overexpression of c-Myc abolished the effect of HEL on energy metabolism

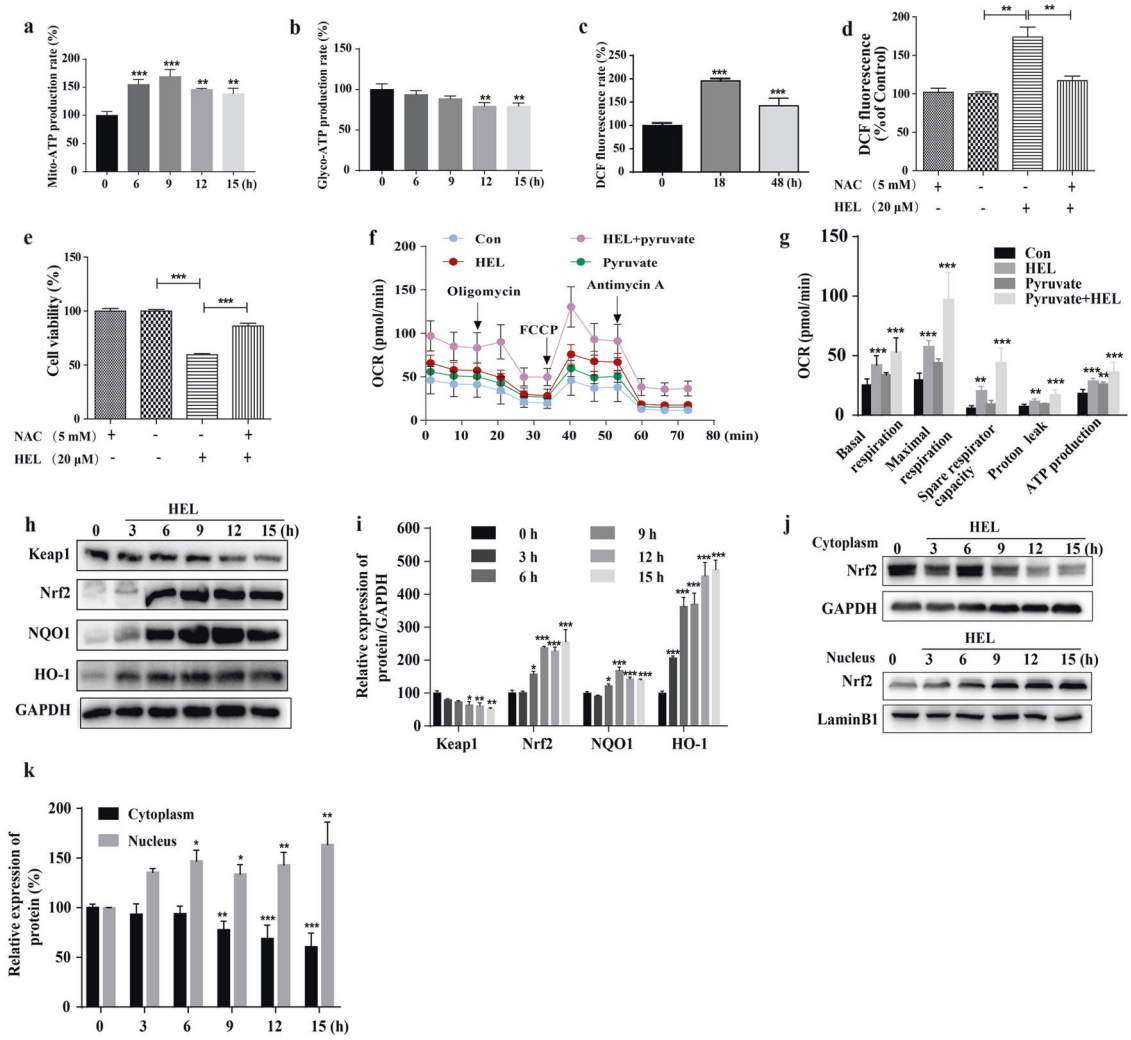

Fig. 3 HEL promotes ROS accumulation in MGC803 cells via enhancing mitochondrial oxidative phosphorylation. a, **b** mitoATP and glycoATP production rates of MGC803 cells treated with HEL (20 μM) for 0, 6, 9, 12, and 15 h. **c** ROS levels in MGC803 cells after HEL treatment for 18 and 48 h. **d** ROS levels in MGC803 cells after HEL treatment with or without NAC pretreatment for 24 h. **e** Cell viability of MGC803 cells after HEL treatment with or without NAC pretreatment for 24 h. **f**, **g** Pyruvate (32 μM) treatment (9 h) significantly increased OCR of HEL-treated MGC803 cells. **h**, **i** Protein expression of Keap1, Nrf2, NQO1, and HO-1 after HEL treatment for 0, 6, 9, 12, and 15 h. **j**, **k** HEL enhanced Nrf2 nuclear translocation in a time-dependent manner. Data are shown as mean ± SD; *$P < 0.05$, **$P < 0.01$; ***$P < 0.001$, compared with Con group or indicated group. $n \geq 3$.

reprogramming in MGC803 cells. As shown in Fig. 4a, b, in MGC803 cells transfected with the LV-Control plasmid, the basal respiration, maximal respiration, spare respiratory capacity, proton leak, and ATP production were increased significantly after HEL treatment ($P < 0.05$, $P < 0.01$, and $P < 0.001$). However, these parameters did not change after HEL treatment in LV-c-Myc plasmid-transfected cells. Similarly, as shown in Fig. 4c, d, although HEL significantly reduced basal and compensatory glycolysis in LV-Control plasmid-transfected MGC803 cells ($P < 0.05$ and $P < 0.01$), it did not change these parameters in LV-c-Myc plasmid-transfected MGC 803 cells. As shown in Fig. 4e, compared with LV-Control plasmid-transfected MGC803 cells, the protein expression of c-Myc and PDHK1 was greatly enhanced in LV-c-Myc plasmid-transfected cells. c-Myc overexpression counteracted HEL-induced inhibition of protein expression of c-Myc and PDHK1 in LV-c-Myc plasmid-transfected cells. Similar results were obtained in SGC7901 cells (Figs. S6a, b and S5c). Furthermore, as shown in Fig. S1a, b, c-Myc siRNA significantly decreased both basal and compensatory glycolysis in MGC 803 cells similarly to HEL, and HEL did not further suppress basal and compensatory glycolysis in c-Myc siRNA-treated MGC803 cells. Additionally, c-Myc siRNA obviously suppressed the protein expression of c-Myc and its target gene PDHK1 similarly to HEL in MGC 803 cells (Fig. S1c). c-Myc siRNA significantly decreased the viability of MGC803 cells similarly to HEL. However, HEL did not further decrease the viability of MGC 803 cells in c-Myc siRNA-treated MGC 803 cells (Fig. S1d), which indicated that HEL inhibited viability of MGC803 cells by suppressing c-Myc. As demonstrated in Fig. S5d and S6c, d, similar results were obtained in SGC7901 cells. Thus, the above results indicated that HEL suppressed glycolysis and the viability of gastric cancer cells by inhibiting c-Myc.

During glucose metabolism in tumor cells, PDHK1 is a gatekeeper that prevents pyruvate from entering mitochondrial OXPHOS [51]. Therefore, inhibition of PDHK1 enhances mitochondrial OXPHOS and reduces glycolysis. As shown in Fig. 4f, g, when PDHK1 was overexpressed in MGC803 cells by transient transfection, the inhibitory effect of HEL on cell viability was abolished. Similar results were obtained in SGC7901 cells (Fig. S5i). These results indicated that HEL inhibited gastric cancer cell growth by

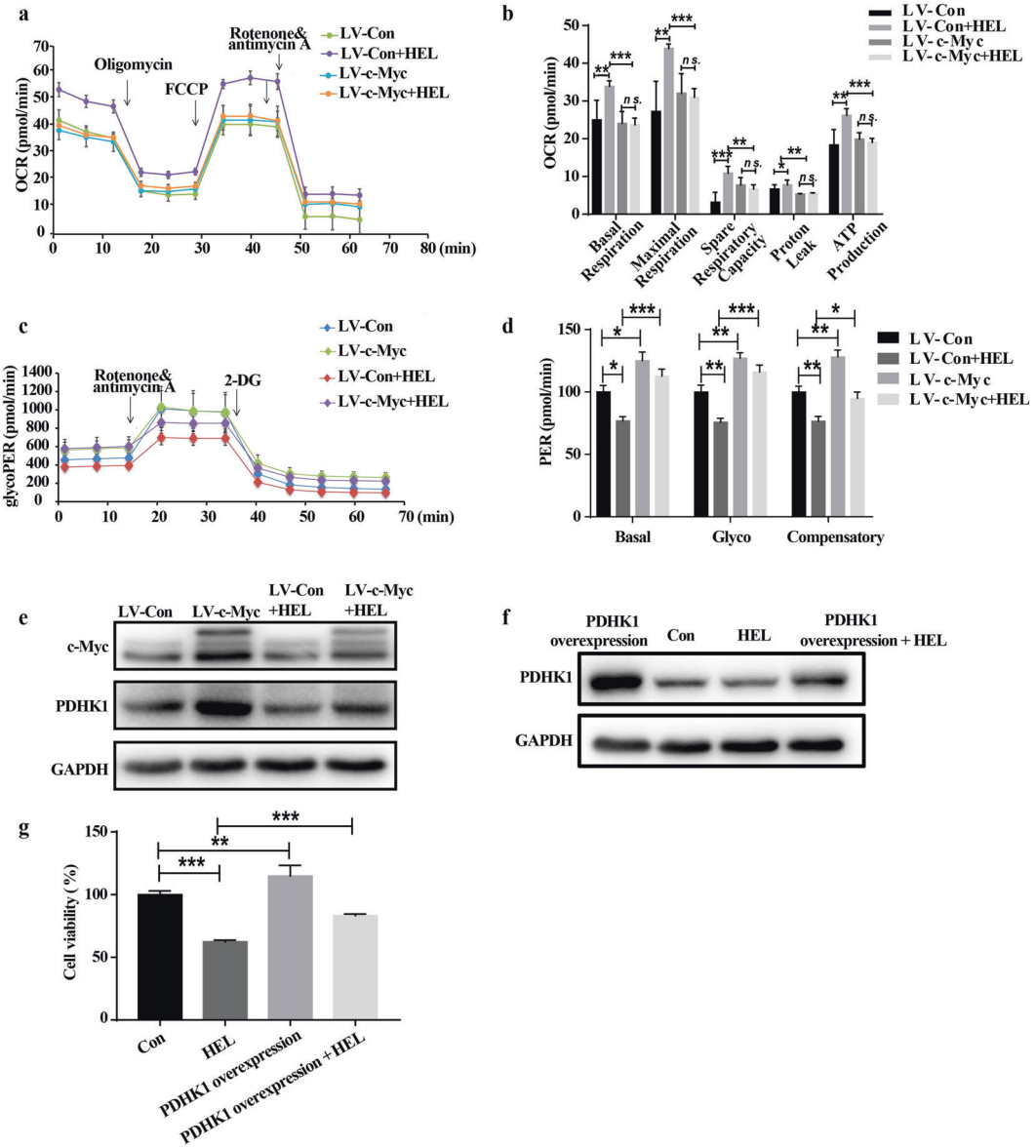

Fig. 4 HEL regulates energy metabolism reprogramming in MGC 803 cells by c-Myc/PDHK1 axis. a, **b** Oxygen consumption rates (OCR) of MGC 803 cells stably overexpressing c-Myc after HEL treatment for 9 h. **c**, **d** Glycolytic rates of MGC803 cells stably overexpressing c-Myc after HEL treatment for 9 h. **e** c-Myc overexpression counteracted the inhibitory effect of HEL on the protein expression of c-Myc and PDHK1 in MGC803 cells. **f** PDHK1 overexpression in MGC803 cells and the inhibitory effect of HEL. **g** Cell viability of MGC803 cells stably overexpressing PDHK1 after HEL treatment for 24 h. Data are shown as mean ± SD; $^{*}P < 0.05$, $^{**}P < 0.01$; $^{***}P < 0.001$, compared with Con group or indicated group. $n \geq 3$.

targeting c-Myc/PDHK1 axis-mediated cancer cell energy metabolism reprogramming.

HEL inhibits c-Myc expression by repressing the mTOR/P70S6K pathway in MGC803 cells. PI3K/Akt/mTOR/P70S6K is an important signaling pathway in regulating c-Myc expression and transcriptional activity [22, 31–33]. As displayed in Fig. 5a, b, HEL treatment, particularly at 20 and 40 μM, inhibited the phosphorylation of PI3K, Akt, mTOR, and P70S6K in MGC803 cells ($P < 0.01$ and $P < 0.001$). To confirm the role of the PI3K/Akt/mTOR/P70S6K pathway in the inhibitory effect of HEL on c-Myc expression and cell viability, the effect of mTOR activator MHY1485 on protein expression of c-Myc and PDHK1 was examined. As shown in Fig. 5c, pretreatment with MHY1485 (14 μM) for 1 h before HEL treatment significantly counteracted the inhibitory effect of HEL on the viability of MGC803 cells. Moreover, pretreatment with MHY1485 partly mitigated the inhibitory effect of HEL on protein expression of c-Myc and PDHK1 in MGC803 cells (Fig. 5d). mTOR inhibitor Rapamycin (Rapa) also significantly inhibited the viability of MGC803 cells similarly to HEL (Fig. S2). Similar results were obtained in SGC7901 cells (Fig. S5h).

As demonstrated in Fig. S7, we further assessed whether PI3K signaling was involved in the inhibitory effect of HEL on the viability of gastric cancer cells. AKT is a very important molecule directly downstream of PI3K signaling. Therefore, SC79 (AKT activator) was used in further experiments. Because SC79 also inhibited the viability of MGC803 cells at >40 μM, we used SC79 at 10 or 20 μM, which had no significant inhibitory effect on the viability of MGC803 cells, but increased phosphorylation of AKT. However, the results from CCK-8 assays demonstrated that SC79 did not reverse the inhibitory effect of HEL on the viability of MGC803 cells, which indicated AKT activation was not involved in

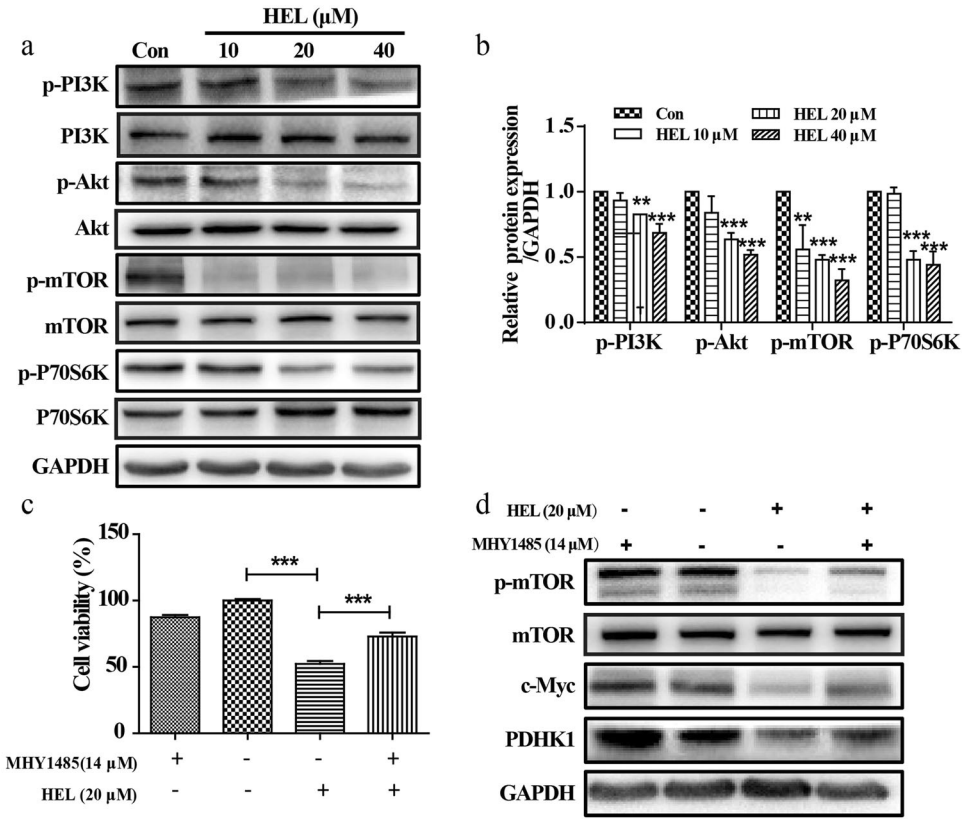

Fig. 5 HEL inhibits c-Myc expression in MGC803 cells by repressing mTOR/P70S6K signaling pathway. a, **b** Protein expression of p-PI3K, p-Akt, p-mTOR, and p-P70S6K in MGC803 cells treated with HEL for 24 h. **c** Cell viability of MGC 803 cells treated with HEL and MHY1485 (14 μM). **d** Protein expression of p-mTOR, c-Myc, and PDHK1 in MGC803 cells treated with HEL and MHY1485 (14 μM). Data are shown as mean ± SD; $^{**}P < 0.01$; $^{***}P < 0.001$, compared with Con group (**b**) or HEL group (**c**). $n \geq 3$.

the inhibitory effect of HEL on the viability of MGC 803 cells, although HEL downregulated the protein expression of p-AKT in MGC 803 cells after treatment for 24 h. Thus, the upstream regulator of mTOR possibly was not PI3K, which will be addressed in our next study.

These results suggested that HEL inhibited gastric cancer cell growth by downregulating the c-Myc/PDHK1 axis through repressing the mTOR/P70S6K signaling pathway in MGC803 cells.

HEL inhibits tumor growth and c-Myc-mediated energy metabolism reprogramming in a MGC803 cell-xenografted mouse model. To verify the inhibitory effect of HEL on gastric cancer growth in vivo, a MGC803 cell-xenografted mouse model was used. As shown in Fig. 6a–d, compared with the control group, HEL (3, 10, and 30 mg/kg) significantly decreased the tumor size and weight without an obvious effect on body weight in nude mice. HEL (3 and 10 mg/kg) decreased the tumor volume as early as day 7 after treatment, and after day 10, HEL (3, 10, and 30 mg/kg) significantly decreased the tumor volume. During the treatment time, HEL showed no significant effect on body weight of nude mice, but 5-Fu significantly decreased body weight from day 13. The tumor inhibition rates of HEL (3, 10, 30 mg/kg) groups were 62.5%, 45.9%, and 51.1%, respectively, whereas that of the 5-Fu group was 78.6%. Consistently, as shown in Fig. 6e, Ki67 immunostaining showed that HEL significantly reduced the expression of Ki67 in tumor tissues compared with untreated tumor tissues in the control group. TUNEL staining revealed that HEL treatment increased the number of apoptotic cells in tumor tissues.

As demonstrated in Fig. 7, HEL treatment (30 mg/kg) decreased the protein expression of Bcl-2 and Ki67, but increased that of cleaved caspase 3 in gastric tumor tissues (Fig. 7a, b, $P < 0.01$ and $P < 0.001$). Moreover, HEL (30 mg/kg) markedly reduced the protein expression of c-Myc, PDHK1, and LDHA (Fig. 7c, d) as well as the phosphorylated PI3K, AKT, mTOR, and p70S6K in tumor tissues (Fig. 7e, f). These results were in agreement with the data from in vitro experiments and suggested that HEL inhibited gastric cancer cell growth in vivo by regulating c-Myc-mediated energy metabolism reprogramming.

DISCUSSION

Aberrant cell metabolism, which is a hallmark of human cancers, plays major roles in cancer progression and chemotherapy [13, 52]. Gastric cancer cells always reprogram their energy metabolism to Warburg-like glucose metabolism [18–20], which indicates that modulation of aberrant energy metabolism is a promising therapeutic approach for cancer treatment. In the present study, HEL effectively inhibited the growth of gastric cancer cell line MGC803 in vitro and in vivo. Further experiments showed that HEL modulated energy metabolism reprogramming in MGC803 and SGC7901 cells by promoting mitochondrial aerobic phosphorylation and reducing glycolysis through suppressing the c-Myc/PDHK1 axis by inhibiting the mTOR/p70S6K signaling pathway, which resulted in excessive accumulation of ROS to inhibit the viability of MGC803 and SGC7901 cells. Our findings suggest that HEL has a prospective therapeutic potential for gastric cancer by targeting cancer cell energy metabolism reprogramming.

The mitochondrion-mediated pathway is an important mechanism of apoptosis. The Bcl-2 family (Bax, Bak and Bim, Bcl-2, Bcl-xL, Bcl-w, and XIAP) promote/inhibit apoptosis by activating cystatin or regulating the release of cytochrome *c* [37]. In the present

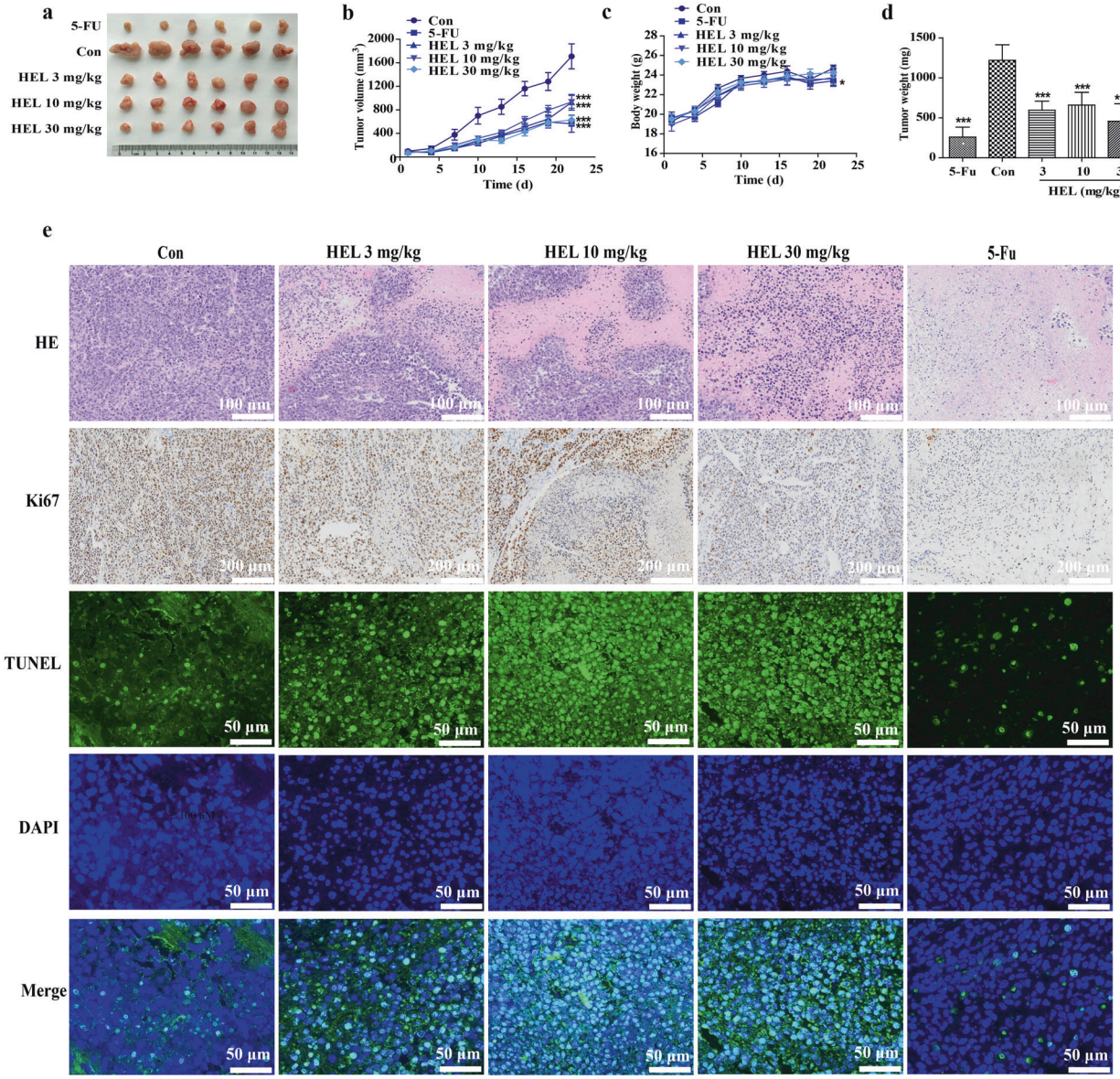

Fig. 6 HEL inhibits tumor growth in the MGC803 cell-xenografted mouse model. a, b Tumor volume changes. **c** Body weight changes. **d** Tumor weight changes. **e** HE, Ki67, and TUNEL staining of tumor tissues. Scale bar for HE staining: 100 μm; for IHC of Ki67: 200 μm; for TUNEL staining: 50 μm. Data are shown as mean ± SD; $^{*}P < 0.05$, $^{***}P < 0.001$, compared with Con group. $n = 6$.

study, HEL induced apoptosis in a dose-dependent manner, downregulated the expression of anti-apoptotic gene Bcl-2, and upregulated the expression of cleaved caspase-3 in vitro and in vivo, which suggests that HEL promoted apoptosis of MGC803 cells via the mitochondrial pathway.

Unlike normal cells, cancer cells prefer to produce energy through glycolysis even in an aerobic environment. A large number of intermediate metabolites and lactic acid are produced through glycolysis with glucose consumption, which meet the needs of rapid proliferation of tumor cells and promote immune escape and tumor metastasis [13, 14, 16–21]. Mitochondrial oxidative phosphorylation is a metabolic pathway that coordinates a series of redox reactions with protein complexes (electron transfer chains) embedded in the inner membrane of mitochondria, which transfers electrons to oxygen and generates ATP and ROS [53]. A low concentration of ROS activates transcription factors to promote cell proliferation and differentiation, but excessive ROS result in cell damage and promote apoptosis [54]. In the present study, HEL significantly enhanced mitochondrial oxidative phosphorylation, reduced aerobic glycolysis, and decreased lactic acid production and efflux in MGC803 and SGC7901 cells. Addition of pyruvate further enhanced HEL-induced mitochondrial OXPHOS in MGC803 cells (9 h), which indicated that HEL significantly enhanced pyruvate transfer into mitochondria for OXPHOS. Consistently, HEL significantly downregulated protein expression of PDHK1 and LDHA in gastric cancer cells in vitro and in vivo. PDP2 is the positive regulator of PDH through dephosphorylating PDH, but PDHK1 is the negative regulator of PDH through phosphorylating PDH [55]. Although PDP2 expression was decreased after HEL treatment, the ratio of p-PDHA1/PDHA1 was still decreased. Therefore, PDH activity was increased by HEL treatment, which indicated the HEL-induced decrease of PDHK1 expression might result in the increased PDH activity of MGC803 cells. It increased mito-ATP production, reduced Glyco-ATP production, and accelerated ROS accumulation in MGC803 cells while enhancing the Nrf2-mediated antioxidant system. The antioxidant NAC abolished HEL-induced ROS accumulation and reversed the inhibitory effect of HEL on the viability

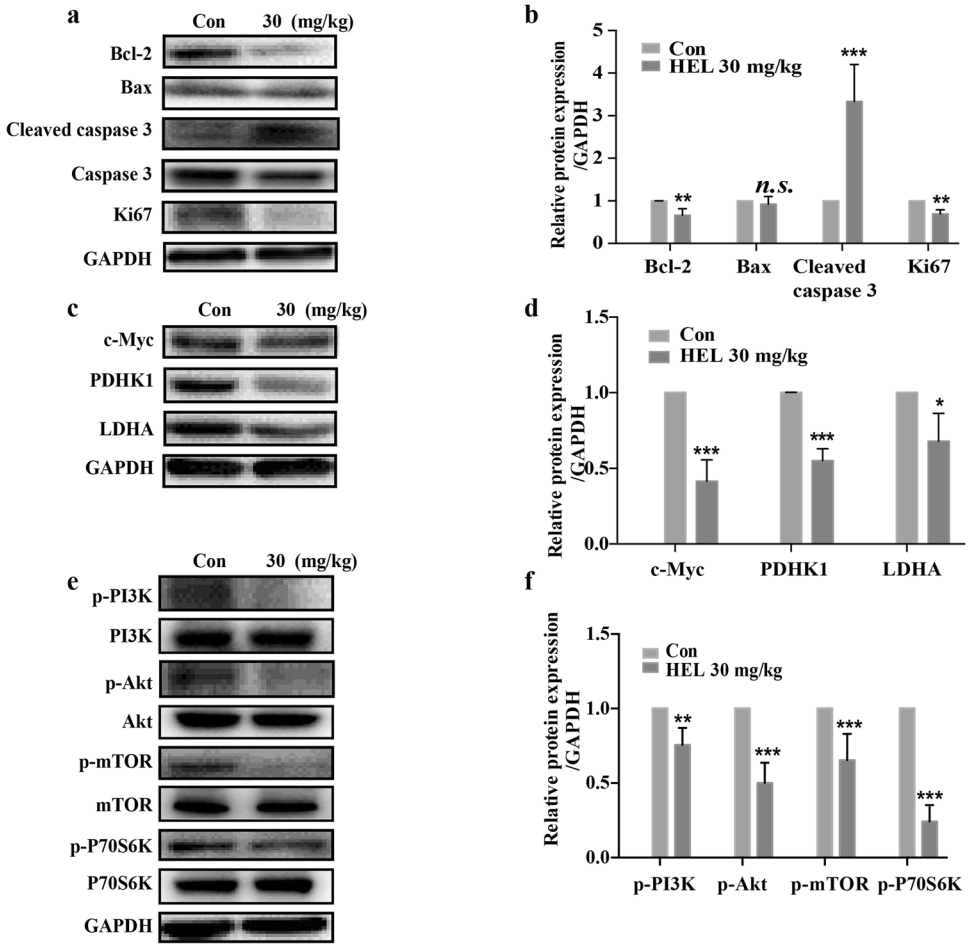

Fig. 7 HEL regulates expression of proteins related with energy metabolism in the MGC803 cell-xenografted mouse model. a, **b** Protein expression of Bcl-2, Bax, cleaved caspase 3, and Ki67 in tumor tissues. **c**, **d** Protein expression of c-Myc, PDHK1 and LDHA in tumor tissues. **e**, **f** Protein expression of p-PI3K, p-Akt, p-mTOR, and p-P70S6K in tumor tissues. Data are shown as mean ± SD; $^{*}P < 0.05$, $^{**}P < 0.01$; $^{***}P < 0.001$, compared with Con group. $n = 6$.

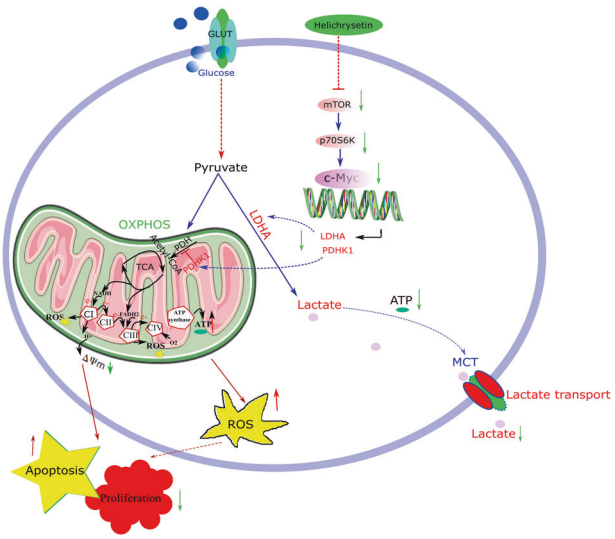

Fig. 8 Schematic illustration of possible underlying mechanism of the inhibition of HEL on gastric cancer cells. HEL suppresses gastric cancer growth via repressing c-Myc/PDHK1 axis-dependent energy metabolic reprogramming through regulation of the mTOR/p70S6K pathway in vitro and in vivo.

of MGC803 cells. However, HEL showed no obvious effect on glucose uptake before cell viability inhibition in MGC803 cells. Therefore, HEL may inhibit gastric cancer cell growth by modulating energy metabolism reprogramming.

Aberrant cell metabolism reprogramming of cancer cell is influenced by transcription factors such as HIF-1α and c-Myc [56]. c-Myc is a proto-oncogene that is strictly regulated at transcriptional and post-transcriptional levels in normal cells but overactivated in cancer cells, which modulates energy metabolism by regulating genes related to energy metabolism [25, 27, 28]. Kim et al. have shown that c-Myc binds to the promoter of PDHK1 and then regulates transcription and expression of PDHK1 [57]. In the present study, HEL significantly inhibited the expression and transcriptional activity of c-Myc in MGC803 cells. When c-Myc was overexpressed, the inhibitory effects of HEL on cell viability and PDHK1, and the modulatory effects on aerobic phosphorylation and glycolysis were abolished in MGC803 and SGC7901 cells. These results indicated that c-Myc/PDHK1 axis-mediated energy metabolism reprogramming played an important role in the antitumor activity of HEL in MGC803 and SGC7901 cells.

The PI3K/Akt/mTOR pathway is a critical pathway for cancer development and progression [58, 59]. Phosphorylation of Akt is increased in many human cancers and PI3K promotes tumorigenesis [58, 60]. mTOR is a downstream molecule in the PI3K/Akt pathway, which is involved in regulating protein synthesis, apoptosis, and energy metabolism [58]. c-Myc regulated by mTOR

is actively involved in mediating cell proliferation, apoptosis, and tumor glucose metabolism [22, 31–33]. In the present study, HEL repressed overactivation of the PI3K/Akt/mTOR/p70S6K signaling pathway in vitro and in vivo. However, the mTOR activator, but not AKT activator, abolished the inhibitory effect of HEL on cell viability and protein expression of c-Myc and PDHK1 in MGC803 cells. Moreover, mTOR inhibitor significantly suppressed the viability and c-Myc expression of MGC803 and SGC7901 cells. These results indicated that AKT activation was not involved in the inhibitory effect of HEL on the viability of MGC803 cells, although HEL downregulated the protein expression of p-AKT in MGC 803 cells after treatment for 24 h. Thus, the upstream regulator of mTOR may not be the PI3K/AKT pathway, which will be addressed in our next study. Therefore, HEL may inhibit gastric cancer growth by suppressing the c-Myc/PDHK1 axis through inhibiting overactivation of the mTOR/p70S6K pathway in MGC803 cells.

CONCLUSIONS

Our study demonstrated that HEL inhibits the viability of gastric cancer cells in vitro and in vivo, probably by modulating c-Myc/PDHK1 axis-mediated cancer energy metabolism reprogramming. We also identified the mTOR/p70S6K pathway as the downstream target of HEL, which reduces c-Myc expression (Fig. 8). These findings suggest that HEL is a potential antitumor drug for gastric cancer patients by targeting energy metabolism reprogramming.

DATA AVAILABILITY

All data that can prove the conclusion of this article are included in the article.

ACKNOWLEDGEMENTS

Special thanks to Prof. Weidong Zhang (SHUTCM) for providing key apparatus for the measurement of mitochondrial energy metabolism. Great thanks to Prof. Jingshan Shen (Shanghai Institute of Materia Medica, Chinese Academy of Sciences, Shanghai, China) for giving us HEL for research.

AUTHOR CONTRIBUTIONS

PW and JMJ did most of experiments and wrote the original draft. XHL took part in finishing cell metabolism assays and Western blotting assay. MZY took part in cell culture and Western blotting assay for manuscript revision. CY took part in cell culture and Western blotting assay. FH and XYF took part in Annexin/PI staining. HW supported to optimize experimental protocols. ZTW and RX gave valuable suggestion for this manuscript. HLS and XJW designed experiments and wrote the manuscript. All authors read and approved the final manuscript.

FUNDING

This work was supported by Shanghai Municipal Natural Science Foundation (21ZR1462800); Educational Commission of Shanghai of China (2020LK014, 18LK015); the National Natural Science Foundation of China (81603354); Graduate Student Innovation Ability Project of Shanghai University of Traditional Chinese Medicine (Y2020030, Y2021088), Shanghai E-research Institute of Bioactive Constituent in TCM plan and the Opening Project of Shanghai Key Laboratory of Compound Chinese Medicines (17DZ2273300).

ADDITIONAL INFORMATION

Supplementary information The online version contains supplementary material available at https://doi.org/10.1038/s41401-021-00750-0.

Competing interests: The authors declare no competing interests.

Ethics approval and consent to participate All animal experiments were carried out in accordance with the protocol approved by the Animal Ethics Committee in Shanghai University of Traditional Chinese Medicine (SHUTCM), which complies with international rules and policies for laboratory animal use and care as founded in the European Community guidelines (EEC Directive of 1986; 86/609/EEC). All animal experiments were approved by the institutional Ethics Committee of SHUTCM (SZY20160914).

REFERENCES

1. Chen W, Zheng R, Baade PD, Zhang S, Zeng H, Bray F, et al. Cancer statistics in China 2015. CA Cancer J Clin. 2016;66:115–32.
2. Global Burden of Disease Cancer Collaboration, Fitzmaurice C, Allen C, Barber RM, Barregard L, Bhutta ZA, et al. Global, regional, and national cancer incidence, mortality, years of life lost, years lived with disability, and disability-adjusted life-years for 32 cancer groups, 1990 to 2015: a systematic analysis for the global burden of disease study. JAMA Oncol. 2017;3:524–48.
3. Siegel RL, Miller KD, Jemal A. Cancer statistics, 2019. CA Cancer J Clin. 2019;69:7–34.
4. Amedei A, Benagiano M, della Bella C, Niccolai E, D'Elios MM. Novel immunotherapeutic strategies of gastric cancer treatment. J Biomed Biotechnol. 2011;2011:437348.
5. Corso G, Roncalli F, Marrelli D, Carneiro F. Roviello F. History, pathogenesis, and management of familial gastric cancer: original study of John XXIII's family. Biomed Res Int. 2013;2013:385132.
6. Nagini S. Carcinoma of the stomach: a review of epidemiology, pathogenesis, molecular genetics and chemoprevention. World J Gastrointest Oncol. 2012;4:156–69.
7. Fujitani K, Yang HK, Mizusawa J, Kim YW, Terashima M, Han SU, et al. Gastrectomy plus chemotherapy versus chemotherapy alone for advanced gastric cancer with a single non-curable factor (REGATTA): a phase 3, randomised controlled trial. Lancet Oncol. 2016;17:309–18.
8. Choi YW, Ahn MS, Jeong GS, Lee HW, Jeong SH, Kang SY, et al. The role of surgical resection before palliative chemotherapy in advanced gastric cancer. Sci Rep. 2019;9:4136.
9. Apicella M, Corso S, Giordano S. Targeted therapies for gastric cancer: failures and hopes from clinical trials. Oncotarget. 2017;8:57654–69.
10. Babiker HM, Mcbride A, Newton M, Boehmer LM, Drucker AG, Gowan M, et al. Cardiotoxic effects of chemotherapy: a review of both cytotoxic and molecular targeted oncology therapies and their effect on the cardiovascular system. Crit Rev Oncol Hematol. 2018;126:186–200.
11. Sun L, Liu J, Yuan Y, Dong Z. Protective effect of the BET protein inhibitor JQ1 in cisplatin-induced nephrotoxicity. Am J Physiol Ren Physiol. 2018;315:F469–78.
12. Fan M, Wen Y, Ye D, Jin Z, Zhao P, Chen D, et al. Acid-responsive H2 -releasing 2D MgB2 nanosheet for therapeutic synergy and side effect attenuation of gastric cancer chemotherapy. Adv Health Mater. 2019;8:e1900157.
13. Hanahan D, Weinberg RA. Hallmarks of cancer: the next generation. Cell. 2011;144:646–74.
14. Granger A, Mott R, Emambokus N. Hacking cancer metabolism. Cell Metab. 2016;24:643–4.
15. Seyfried TN, Shelton LM. Cancer as a metabolic disease. Nutr Metab. 2010;7:7.
16. Gatenby RA, Gillies RJ. Why do cancers have high aerobic glycolysis? Nat Rev Cancer. 2004;4:891–9.
17. Vander Heiden MG, Cantley LC, Thompson CB. Understanding the Warburg effect: the metabolic requirements of cell proliferation. Science. 2009;324:1029–33.
18. Liu J, Pan C, Guo L, Wu M, Guo J, Peng S, et al. A new mechanism of trastuzumab resistance in gastric cancer: MACC1 promotes the Warburg effect via activation of the PI3K/AKT signaling pathway. J Hematol Oncol. 2016;9:76.
19. Liu L, Wang Y, Bai R, Yang K, Tian Z. MiR-186 inhibited aerobic glycolysis in gastric cancer via HIF-1α regulation. Oncogenesis. 2016;5:e224.
20. Gao S, Chen M, Wei W, Zhang X, Zhang M, Yao Y, et al. Crosstalk of mTOR/PKM2 and STAT3/c-Myc signaling pathways regulate the energy metabolism and acidic microenvironment of gastric cancer. J Cell Biochem. 2019;120:1193–202.
21. Ganapathy-Kanniappan S. Molecular intricacies of aerobic glycolysis in cancer: current insights into the classic metabolic phenotype. Crit Rev Biochem Mol Biol. 2018;53:667–82.
22. Gustafson WC, Weiss WA. Myc proteins as therapeutic targets. Oncogene. 2010;29:1249–59.
23. Zheng L, Liang X, Li S, Li T, Shang W, Ma L, et al. CHAF1A interacts with TCF4 to promote gastric carcinogenesis via upregulation of c-MYC and CCND1 expression. EBioMedicine. 2018;38:69–78.
24. Dang CV, Le A, Gao P. MYC-induced cancer cell energy metabolism and therapeutic opportunities. Clin Cancer Res. 2009;15:6479–83.
25. Kim JW, Gao P, Liu YC, Semenza GL, Dang CV. Hypoxia-inducible factor 1 and dysregulated c-Myc cooperatively induce vascular endothelial growth factor and metabolic switches hexokinase 2 and pyruvate dehydrogenase kinase 1. Mol Cell Biol. 2007;27:7381–93.
26. Shim H, Dolde C, Lewis BC, Wu CS, Dang G, Jungmann RA, et al. c-Myc transactivation of LDHA: implications for tumor metabolism and growth. Proc Natl Acad Sci USA. 1997;94:6658–63.

27. Osthus RC, Shim H, Kim S, Li Q, Reddy R, Mukherjee M, et al. Deregulation of glucose transporter 1 and glycolytic gene expression by c-Myc. J Biol Chem. 2000;275:21797–800.
28. Li F, Wang Y, Zeller KI, Potter JJ, Wonsey DR, O'Donnell KA, et al. Myc stimulates nuclearly encoded mitochondrial genes and mitochondrial biogenesis. Mol Cell Biol. 2005;25:6225–34.
29. Miller DM, Thomas SD, Islam A, Muench D, Sedoris K. c-Myc and cancer metabolism. Clin Cancer Res. 2012;18:5546–53.
30. Kim JW, Tchernyshyov I, Semenza GL, Dang CV. HIF-1-mediated expression of pyruvate dehydrogenase kinase: a metabolic switch required for cellular adaptation to hypoxia. Cell Metab. 2006;3:177–85.
31. Masui K, Tanaka K, Akhavan D, Babic I, Gini B, Matsutani T, et al. mTOR complex 2 controls glycolytic metabolism in glioblastoma through FoxO acetylation and upregulation of c-Myc. Cell Metab. 2013;18:726–39.
32. Zhang X, Chen J, Ai Z, Zhang Z, Lin L, Wei H. Targeting glycometabolic reprogramming to restore the sensitivity of leukemia drug-resistant K562/ADM cells to adriamycin. Life Sci. 2018;215:1–10.
33. Allen-Petersen BL, Risom T, Feng Z, Wang Z, Jenny ZP, Thoma MC, et al. Activation of PP2A and inhibition of mTOR synergistically reduce MYC signaling and decrease tumor growth in pancreatic ductal adenocarcinoma. Cancer Res. 2019;79:209–19.
34. Ali MS, Tezuka Y, Awale S, Banskota AH, Kadota S. Six new diarylheptanoids from the seeds of *Alpinia blepharocalyx*. J Nat Prod. 2001;64:289–93.
35. Vogel S, Ohmayer S, Brunner G, Heilmann J. Natural and non-natural prenylated chalcones: synthesis, cytotoxicity and anti-oxidative activity. Bioorg Med Chem. 2008;16:4286–93.
36. Hua SZ, Wang XB, Luo JG, Wang JS, Kong LY. A pair of unique sesquiterpene-chalcone conjugates isolated from the seeds of *Alpinia katsumadai*. Tetrahedron Lett. 2008;49:5658–61.
37. Lopez J, Tait SWG. Mitochondrial apoptosis: killing cancer using the enemy within. Br J Cancer. 2015;112:957–62.
38. Ho YF, Karsani SA, Yong WK, Abd, Malek SN. Induction of apoptosis and cell cycle blockade by helichrysetin in A549 human lung adenocarcinoma cells. Evid Based Complement Altern Med. 2013;2013:857257.
39. Fong HY, Malek SNA, Yee HS. Helichrysetin induces DNA damage that triggers JNK-mediated apoptosis in Ca Ski cells. Pharmacogn Maq. 2017;13:607–12.
40. Wang Q, Huang J, Ma K, Li T, Chen M, Wang S, et al. Evaluation of ghost cell survival in the area of radiofrequency ablation. PLoS One. 2012;7:e53158.
41. Shi HL, Liu CH, Ding LL, Zheng Y, Fei XY, Lu L, et al. Alterations in serotonin, transient receptor potential channels and protease-activated receptors in rats with irritable bowel syndrome attenuated by Shugan decoction. World J Gastroenterol. 2015;21:4852–63.
42. Shi J, Qu Y, Li X, Sui F, Yao D, Yang Q, et al. Increased expression of EHF via gene amplification contributes to the activation of HER family signaling and associates with poor survival in gastric cancer. Cell Death Dis. 2016;7:e2442.
43. Szafarowski T, Sierdzinski J, Szczepanski MJ, Whiteside TL, Ludwig N, Krzeski A. Microvessel density in head and neck squamous cell carcinoma. Eur Arch Otorhinolaryngol. 2018;275:1845–51.
44. Zhu X, Lei X, Wang J, Dong W. Protective effects of resveratrol on hyperoxia-induced lung injury in neonatal rats by alleviating apoptosis and ROS production. J Matern Fetal Neonatal Med. 2020;33:4150–8.
45. Li H, Wang P, Huang F, Jin J, Wu H, Zhang B, et al. Astragaloside IV protects blood-brain barrier integrity from LPS-induced disruption via activating Nrf2 antioxidant signaling pathway in mice. Toxicol Appl Pharmacol. 2018;340:58–66.
46. Kensler TW, Wakabayashi N, Biswal S. Cell survival responses to environmental stresses via the Keap1-Nrf2-ARE pathway. Annu Rev Pharmacol Toxicol. 2007;47:89–116.
47. Wei Y, Gong J, Xu Z, Thimmulappa RK, Mitchell KL, Welsbie DS, et al. Nrf2 in ischemic neurons promotes retinal vascular regeneration through regulation of semaphorin 6A. Proc Natl Acad Sci USA. 2015;112:6927–36.
48. McSweeney SR, Warabi E, Siow RC. Nrf2 as an endothelial mechanosensitive transcription factor: going with the flow. Hypertension. 2016;67:20–9.
49. Shang Y, Zhou Q, Wang T, Jiang Y, Zhong Y, Qian G, et al. Airborne nitro-PAHs induce Nrf2/ARE defense system against oxidative stress and promote inflammatory process by activating PI3K/Akt pathway in A549 cells. Toxicol Vitr. 2017;44:66–73.
50. Jaramillo MC, Zhang DD. The emerging role of the Nrf2-Keap1 signaling pathway in cancer. Genes Dev. 2013;27:2179–91.
51. Kroemer G, Dallaporta B, Resche-Rigon M. The mitochondrial death/life regulator in apoptosis and necrosis. Annu Rev Physiol. 1998;60:619–42.
52. Zhu J, Wu G, Song L, Cao L, Tan Z, Tang M, et al. NKX2-8 deletion-induced reprogramming of fatty acid metabolism confers chemoresistance in epithelial ovarian cancer. EBioMedicine. 2019;43:238–52.
53. Volobueva A, Melnichenko A, Grechko A, Orekhov AN. Mitochondrial genome variability: the effect on cellular functional activity. Ther Clin Risk Manag. 2018;14:237–45.
54. Leanza L, Romio M, Becker KA, Azzolini M, Trentin L, Managò A, et al. Direct pharmacological targeting of a mitochondrial ion channel selectively kills tumor cells in vivo. Cancer Cell. 2017;31:516–31.
55. Piccinini M, Mostert M, Alberto G, Ramondetti C, Novi RF, Dalmasso P, et al. Down-regulation of pyruvate dehydrogenase phosphatase in obese subjects is a defect that signals insulin resistance. Obes Res. 2005;13:678–86.
56. Gordan JD, Thompson CB, Simon MCHIF. and c-Myc: sibling rivals for control of cancer cell metabolism and proliferation. Cancer Cell. 2007;12:108–13.
57. Kim J, Gao P, Liu YC, Semenza GL, Dang CV. Hypoxia-inducible factor 1 and dysregulated c-Myc cooperatively induce vascular endothelial growth factor and metabolic switches hexokinase 2 and pyruvate dehydrogenase kinase 1. Mol Cell Biol. 2007;27:7381–93.
58. Laplante M, Sabatini DM. mTOR signaling in growth control and disease. Cell. 2012;149:274–93.
59. Di Conza G, Trusso Cafarello S, Loroch S, Mennerich D, Deschoemaeker S, Di Matteo M, et al. The mTOR and PP2A pathways regulate PHD2 phosphorylation to fine-tune HIF1α levels and colorectal cancer cell survival under hypoxia. Cell Rep. 2017;18:1699–712.
60. Martini M, De Santis MC, Braccini L, Gulluni F, Hirsch E. PI3K/AKT signaling pathway and cancer: an updated review. Ann Med. 2014;46:372–83.